Articles
doi.org/10.1002/batt.202000050

Chemistry Europe
European Chemical Societies Publishing

Special Collection

A 4.8 V Reversible Li_2CoPO_4F/Graphite Battery Enabled by Concentrated Electrolytes and Optimized Cell Design

Seongjae Ko,[a] Yuki Yamada,*[a, b] and Atsuo Yamada[a, b]

Elevating the voltage of lithium-ion batteries (currently 3.8 V) is a simple and pragmatic way to achieve high-density energy storage. Many so-called "5 V-class" cathodes have been discovered over the past decade; however, they have been studied below 5 V (*vs.* Li/Li^+) because of the severe oxidation of electrolytes and other cell components. Here, highly reversible charge-discharge cycling of Li_2CoPO_4F/graphite full-cells up to a cut-off voltage of 5.2 V is demonstrated for the first time. This result is achieved with synergetic effects of an optimized cell design and a newly designed concentrated electrolyte based on $LiBF_4$, propylene carbonate (PC), and fluoroethylene carbonate (FEC). As an electrolyte design rationale, two important properties of high oxidation stability and anode-passivation ability are clearly allocated for $LiBF_4$ and FEC, respectively. Besides, all other cell components (e.g., conductive carbon, separator, and binder) are reconsidered and customized for use at >5 V. The new concentrated electrolyte and optimized cell design presented here will pave the way for developing over-5 V rechargeable batteries.

1. Introduction

Li-ion batteries have become a dominant energy-storage source for portable electronic devices, electric vehicles, and energy storage systems (ESSs).[1] However, the rapidly increasing energy demand requires high-energy-density Li-ion batteries.[2,3] As a simple and practical approach, increasing the voltage of Li-ion batteries (currently 3.8 V) with 5 V-class cathode materials has been studied over the past decade. In most cases, however, the so-called "5 V-class" Li-ion batteries have been studied in potential ranges under 5 V *vs.* Li/Li^+.[4–7] Higher-potential cathodes with a potential plateau over 5 V *vs.* Li/Li^+ (e.g., olivine $LiNiPO_4$, spinel $LiCoMnO_4$, and fluorinated olivine Li_2CoPO_4F) have been reported to show poor charge-discharge reversibility.[4–7] This is because the highly oxidizing conditions over 5 V significantly degrade electrolytes, cathode materials, and other cell components.[5,6,8] Thus, a totally new battery design employing an oxidation-tolerant electrolyte and other components is required to realize true 5 V-class Li-ion batteries.

A conventional approach to developing oxidation-tolerant electrolytes is to employ fluorinated solvents (e.g., fluoroethylene carbonate (FEC)).[9–11] Fluorinated solvents generally have low highest occupied molecular orbital (HOMO) levels, and thus exhibit higher oxidation stability; however, the long-term cycling performance of full-cells with graphite anodes is unsatisfactory due to transition metal dissolution.[9–11] On the other hand, the concept of salt-concentrated electrolytes ($>3\ mol\ dm^{-3}$ (M)) has recently emerged as a promising way of realizing high-voltage batteries.[12–20] In essence, their unique coordination structures consisting of anion-cation-solvent networks can enhance oxidation stability due to the downward shift of the solvent molecule HOMO levels and can also impede the dissolution of transition metal from the cathode, thus leading to better cycling performance.[13,17,21–23] Two types of concentrated electrolytes, amide salt-based (e.g., $LiF(SO_2F)_2$ (LiFSA)) and $LiBF_4$ salt-based systems, have been studied thus far. Concentrated LiFSA electrolytes enable stable cycling of anodes due to the formation of the FSA anion-derived solid electrolyte interphase (SEI).[17,21–23] However, these amide salt-based electrolytes are not suitable for higher-voltage cells that operate over 5 V due to the low electrochemical stability of the salt itself (<5.2 V *vs.* Li/Li^+) and poor passivating ability with the aluminum current collectors.[18,24,25]

The challenges when working in a highly oxidizing environment are not limited to the electrolyte, and the disintegration of other cell components, including separators, binders, and carbon conductive agents must also be considered synthetically. However, to date, these various design parameters for high-voltage cells have mostly been studied separately at working potentials below 5 V *vs.* Li/Li^+.[5,6,8]

Herein, we report a new concentrated electrolyte of $LiBF_4$/propylene carbonate (PC): FEC, coupled with an optimized cell design, that successfully resolves the issues above. We selected $LiBF_4$ instead of amide salts, because $LiBF_4$ has a high oxidation stability and can prevent aluminum corrosion.[14–16,26,27] As for solvent, we selected PC with a high oxidation stability and a low melting point, and FEC with a high SEI-forming ability toward the anode (Figure 1). We demonstrate stable 700 charge-discharge cycles of Li_2CoPO_4F/graphite full-cells at a

[a] S. Ko, Dr. Y. Yamada, Prof. A. Yamada
Department of Chemical System Engineering
The University of Tokyo
7-3-1, Hongo, Bunkyo-ku, Tokyo 113-8656, Japan
E-mail: yamada@chemsys.t.u-tokyo.ac.jp
[b] Dr. Y. Yamada, Prof. A. Yamada
Elements Strategy Initiative for Catalysts & Batteries (ESICB)
Kyoto University
1-30, Goryo-Ohara, Nishikyo-ku, Kyoto 615-8245, Japan

Supporting information for this article is available on the WWW under https://doi.org/10.1002/batt.202000050

Special Collection *An invited contribution to a Special Collection on Electrolytes for Electrochemical Energy Storage*

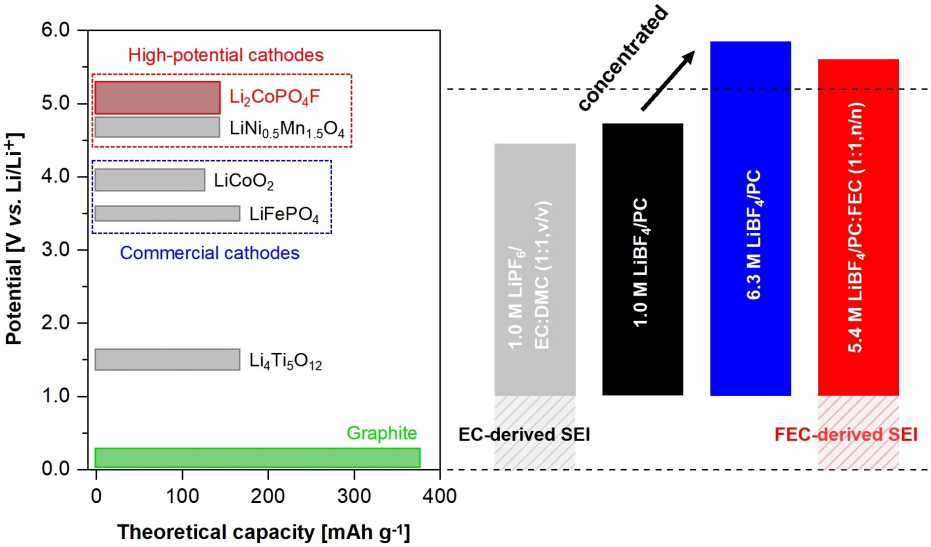

Figure 1. A scheme showing the electrochemical stability window of the electrolytes. The concentrated $LiBF_4$/PC electrolyte exhibits high oxidation stability, but it cannot form a stable SEI on a graphite anode. On the other hand, owing to the formation of an FEC-derived SEI, the concentrated $LiBF_4$/PC:FEC electrolyte can cover the working potentials of both Li_2CoPO_4F and graphite, thus enabling the reversible cycling of a Li_2CoPO_4F/graphite full-cell

slow constant rate (0.5 C-rate) with an upper cut-off voltage of 5.2 V, overcoming much higher oxidative environments than those of well-studied $LiNi_{0.5}Mn_{1.5}O_4$/graphite full-cells generally cycled below 5 V. We believe that the proposed electrolyte and advanced cell design will be a crucial foundation for hitherto-undeveloped over-5-V-class batteries.

2. Results and Discussion

2.1. Oxidation Stability and Solution Structures

The oxidation stability of an electrolyte is of primary importance in ensuring the high-voltage operation of batteries. Figure 2a shows the oxidation stability on a Pt electrode. We found that a high salt concentration significantly enhances oxidative stability. In concentrated 6.3 M $LiBF_4$/PC (salt:solvent = 1:1.3, n/n), the anodic current started to flow at 5.7 V (*vs.* Li/Li^+), which was far higher than that in dilute 1.0 M $LiBF_4$/PC (salt:solvent = 1:11.3, n/n) and commercial 1.0 M $LiPF_6$/EC:DMC (1:1, v/v) (Figure 2a and Figure S3). As shown for the 5.4 M $LiBF_4$/PC:FEC (1:1, n/n) (salt:solvent = 1:1.8, n/n), the introduction of FEC slightly degraded the oxidation stability, but the system still had sufficient stability for the reaction potential of Li_2CoPO_4F (> 5.3 V *vs.* Li/Li^+) (Figure 2a).

To clarify the mechanism behind the enhanced oxidative stability, the solution structures of the $LiBF_4$/PC electrolytes were studied *via* Raman spectroscopy (Figure 2b and Figure S4). A free PC molecule shows a ring-deformation band at 716 cm^{-1}, and the band shifts upwards to 723 cm^{-1} when solvating Li^+.[28] With the increasing salt concentration, the peak intensity for the solvating PC molecules increased at the expense of the peak for free PC molecules (Figure 2b and Figure S4). Simultaneously, the vibration band of BF_4^- also shifted upward from 767 cm^{-1} to 780 cm^{-1}, suggesting extensive ion pairing of Li^+ and BF_4^- to form contact ion pairs (CIPs, BF_4^- coordinating to one Li^+) and aggregate clusters (AGGs, BF_4^- coordinating to two or more Li^+) (Figure S4).[29] For the most concentrated 6.3 M $LiBF_4$/PC electrolyte, almost all PC molecules and BF_4^- anions were coordinated to Li^+ to form AGGs. The coordination of the PC molecule to Li^+ (a strong Lewis acid or electron acceptor) induces a partial donation of an electron from the PC molecule to Li^+, which lowers its HOMO level and thus enhances its oxidation stability.[30] This effect is also applied to BF_4^- in the AGGs to enhance its oxidation stability. Furthermore, the enhanced oxidation stability brings about another merit in high-voltage batteries. It is known that the coexistence of BF_4^- and PC generates HF upon oxidation by H-abstraction from PC and F-abstraction from BF_4^-.[31] However, both the H- and F-abstraction reactions can be retarded in concentrated electrolyte because both PC and BF_4^- have higher oxidation stability when coordinated to Li^+. As shown in Figure 2b and Figure S5, the introduction of FEC did not change the coordination state of PC or BF_4^-, which accounts for the high oxidation stability of 5.4 M $LiBF_4$/PC:FEC (1:1, n/n).

The enhanced oxidation stability enabled highly reversible cycling of Li_2CoPO_4F up to a 5.2 V cut-off with an average Coulombic efficiency of ~99% for 100 cycles (Figure S6). Notably, concentrated LiFSA electrolytes (e.g., 5.5 M LiFSA/DMC), which show excellent cycling stabilities with a $LiNi_{0.5}Mn_{1.5}O_4$ cathode, exhibited a lower Coulombic efficiency with the Li_2CoPO_4F cathode than the present $LiBF_4$ electrolytes (Figure S7).[13,17,18] This difference is because such amide salts possess a lower oxidation stability (< 5 V *vs.* Li/Li^+) and poorer passivation ability toward the Al current collector than $LiBF_4$.[18,24,25] Hence, $LiBF_4$-based concentrated electrolytes are more suitable when applied to high-potential cathodes exceeding 4.5 V.

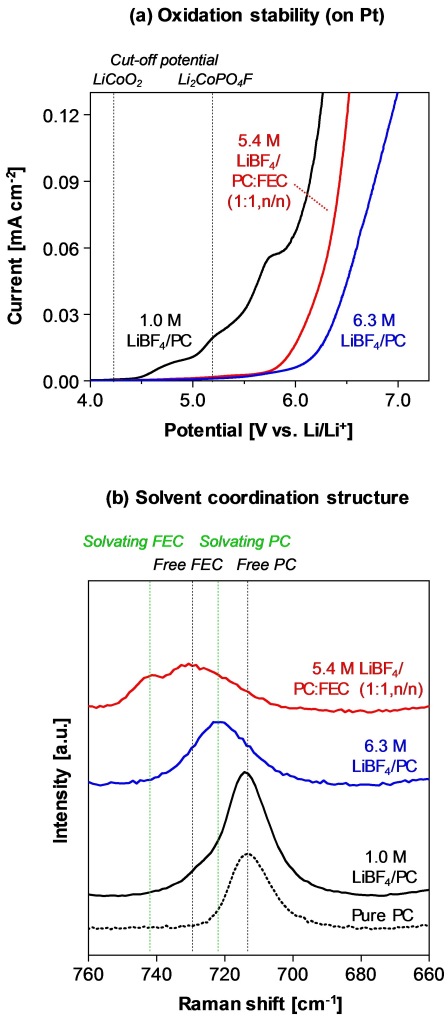

Figure 2. Oxidation stability and solution structures of the dilute and concentrated $LiBF_4$ electrolytes. a) Linear sweep voltammogram of the Pt electrode at a scan rate of 0.1 $mV s^{-1}$. b) Raman spectra of electrolyte solutions in the range of 660–760 cm^{-1}, corresponding to the ring-deformation mode of the solvents: free PC (716 cm^{-1}), solvating PC (723 cm^{-1}), free FEC (729 cm^{-1}), and solvating FEC (742 cm^{-1}). The intensified coordination between PC and Li^+ in the concentrated $LiBF_4$ electrolytes is represented by the absence of free PC molecules, which is crucial for enhancing the oxidative stability of the electrolyte.

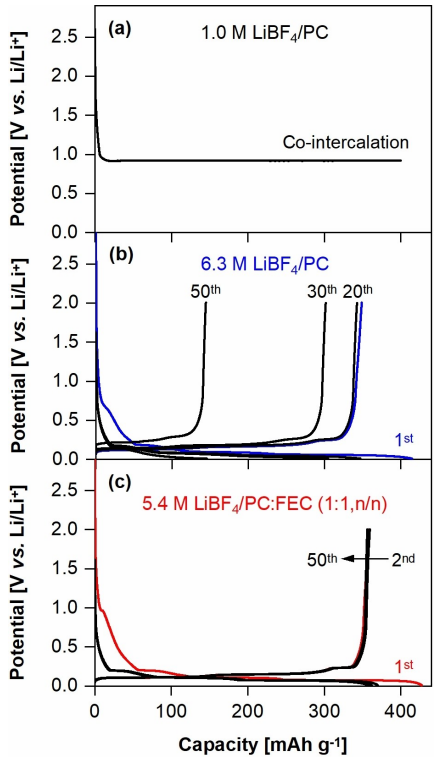

Figure 3. Passivation ability of the dilute and concentrated $LiBF_4$ electrolytes evaluated with natural graphite/Li half-cells. Charge and discharge curves of the cells with a) 1.0 M $LiBF_4$/PC, b) 6.3 M $LiBF_4$/PC, and c) 5.4 M $LiBF_4$/PC:FEC (1:1, n/n) electrolytes. The passivation ability was significantly enhanced with the introduction of FEC. The loading level of the graphite electrodes was 1.0–1.5 $mg cm^{-2}$. A glass fiber separator was used.

2.2. Anode Passivation and Introduction of FEC

Before conducting the full-cell test, the anode-passivation ability of the electrolytes was evaluated with natural graphite/Li half-cells. When 1.0 M $LiBF_4$/PC was applied, the co-intercalation of Li^+ and PC, accompanied by the exfoliation of the graphene layers, was observed during the first charge at 0.9 V (Figure 3a).[32] On the other hand, 6.3 M $LiBF_4$/PC could suppress the co-intercalation to enable reversible Li^+ intercalation (Figure 3b), which agrees with previous reports.[18,22,33–35] This effect has been attributed to i) salt-derived SEI formation resulting from the unique AGG-predominant solution structure and/or ii) upward shift of the Li^+ intercalation potential over that of the co-intercalation resulting from high Li^+ activity.[34,36–40] However, for the present 6.3 M $LiBF_4$/PC electrolyte, the discharge capacity drastically decreased after 20 cycles (Figure 3b and Figure S8), which is in stark contrast to the long-term stable cycling demonstrated in concentrated LiFSA and $LiN(SO_2CF_3)_2$ (LiTFSA) electrolytes.[13,17,18] This difference indicates that the $LiBF_4$-derived SEI is less stable than the LiFSA- or LiTFSA-derived SEI. To strengthen the SEI, we introduced FEC as a complementary SEI-forming component. As shown in Figure 3c and Figure S8, 5.4 M $LiBF_4$/PC:FEC (1:1, n/n) exhibited stable charge and discharge over 100 cycles. Therefore, this electrolyte provides a wide potential window of 0~5.3 V that enables the reversible reactions of both Li_2CoPO_4F and graphite.

2.3. Cell Design for High-voltage Batteries

In addition to applying a new electrolyte, we reconsidered all other cell components to minimize unfavorable side reactions over 5 V. First, a polymer-based binder, lithiated polyacrylic acid (LiPAA), was selected for the cathode, which enabled higher reversibility for Li_2CoPO_4F/Li half-cells than conventional polyvinylidene difluoride (PVDF) or sodium carboxymethyl cellulose (NaCMC) (Figure S9). The better performance is owing to its higher adhesion force and lower swelling properties, leading to better electrical contact between the cathode and current collector.[41] Besides, LiPAA functions as an artificial passivation film to suppress the oxidation of electrolyte and the

dissolution of transition metal from the cathode.[41] Second, a quartz fiber separator was adopted instead of a conventional polypropylene (PP) separator (Figure S10). The quartz (SiO_2) functions as an HF scavenger to minimize the negative effect of HF on both the cathode and anode.[42] Besides, additional heat treatment over 800 °C in Ar removes water molecules, hydroxyl groups (silanol defects), and impurities on the SiO_2 surface, leading to higher reversibility of Li_2CoPO_4F/Li half-cells (Figure S10). Third, the conductive carbon (acetylene black) for the cathode was heated at 1100 °C in an Ar atmosphere. This procedure can minimize oxygen functional groups and absorbed water molecules on the carbon surface, which cause various side reactions with electrolyte at high potentials.[43–45] Finally, tetraethyl orthosilicate (TEOS) was added to the cathode slurry to obtain 5 wt% SiO_2-coated cathode, which can suppress the oxidation of electrolyte on the cathode at high potentials.[46] The cyclic voltammograms of Li_2CoPO_4F in the standard and optimized cells with commercial electrolytes are shown in Figure 4. The peaks of Li_2CoPO_4F represent the extraction/insertion of Li^+ from several Li sites in its crystal lattice with changing valance states of Co.[46] So far, only two oxidation peaks (Li^+ de-intercalation) with one broad reduction peak (Li^+ intercalation) have been reported experimentally.[47–50] However, our optimized cell design allows us to observe four sharp redox pairs at 4.8/4.7, 4.9/4.8, 5.1/5.0, and 5.3/5.1 V (*vs.* Li/Li^+), for the first time. A previous theoretical work predicted a three-step reaction of Li_2CoPO_4F, but the observation of four redox pairs suggests another reaction mechanism.[51] Superior reversibility of the optimized cell design was also demonstrated in the charge-discharge tests of Li_2CoPO_4F/Li half-cells (Figure S11) and Li_2CoPO_4F/graphite full-cells (Figure S12) with commercial electrolyte.

2.4. 5.2 V Cut-Off Cycling of Li_2CoPO_4F/Graphite Full-Cells

Together with these total cell optimizations, 5.4 M $LiBF_4$/PC:FEC (1:1, n/n) electrolyte enabled, for the first time, highly reversible charge-discharge cycling of a Li_2CoPO_4F/graphite full-cell up to a 5.2 V cut-off at 0.5 C-rate (Figure 5a). Owing to the increased cut-off voltage, a high reversible capacity of 112 mAh g^{-1} (on the weight basis of Li_2CoPO_4F) was achieved at an average cell voltage of 4.8 V (Figure 5a and Figure S13). The mixing ratio of PC and FEC also influenced the cycling performance (Figure S14), suggesting room for further optimization of the electrolyte. Noticeably, using 5.9 M $LiBF_4$/PC:FEC (7:3, n/n), the capacity retention after 700 cycles was approximately 70% and average Coulombic efficiency was 99.6% for 700 cycles (Figure 5a and Figure S14), which are the highest for such 5 V-class batteries.

In general, the dissolution of transition metals is responsible for the structural degradation of cathode materials as well as the increase in the resistance at the anode surface in a full-cell, thus provoking a severe capacity drop, especially for high-voltage operation.[4–7] The energy-dispersive X-ray spectroscopy (EDX) measurements indicated a high content of Co on the graphite anode collected from the cycled full-cell in 1.0 M $LiPF_6$/EC:DMC (1:1, v/v), while the content was negligible in concentrated 5.4 M $LiBF_4$/PC:FEC (1:1, n/n) (Figure 5b). This difference can be explained with the advanced design of both the electrode and electrolyte. First, the optimized cathode with LiPAA binder, quart separator, and SiO_2 coating, contributes to not only blocking the direct contact between the electrode and electrolyte, but also preventing the HF generation.[41,42,46,47] Thus, the surface damage of the cathode material at high potentials could be mitigated. Moreover, two distinct features of the concentrated $LiBF_4$/PC:FEC help to prevent the transition metal dissolution from the cathode material. First, the BF_4^- anion, which has a higher thermal and chemical stability than PF_6^-, reduces the generation of HF acid, thus preventing

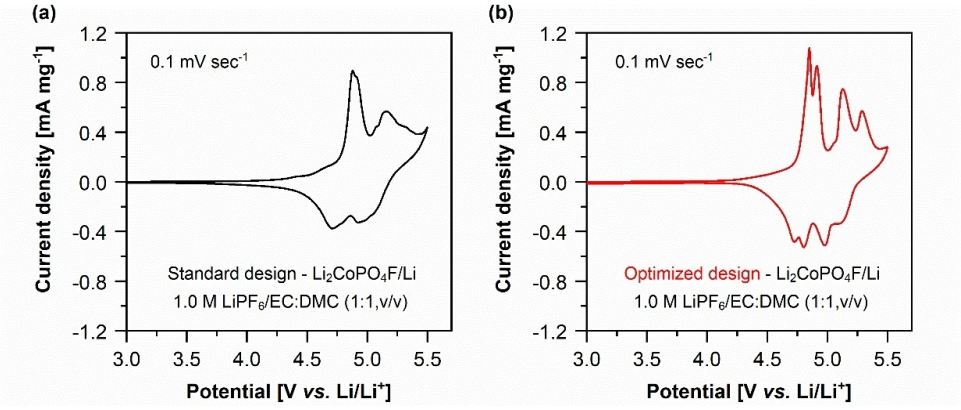

Figure 4. Optimization of cell components. Cyclic voltammograms of Li_2CoPO_4F/Li half-cells with a) standard and b) optimized design. a) The cell with standard design using PP separator and a cathode consisting 85 wt% Li_2CoPO_4F/pristine AB composite, 10 wt% pristine AB, and 5 wt% PVDF. The cathode for the standard design was dried at 120 °C for 12 h under vacuum. b) The cell with optimized design using heated quartz fiber separator and a cathode including 85 wt% Li_2CoPO_4F/annealed AB composite, 10 wt% annealed AB, and 5 wt% LiPAA. TEOS was applied to obtain 5 wt% SiO_2-coated electrode. The drying condition of the cathode for the optimized design was 200 °C for 1 h under vacuum. In both standard and optimized conditions, the commercial electrolyte 1.0 M $LiPF_6$/EC:DMC (1:1, v/v) was used. The tests were conducted in the potential range 5.5–3.0 V (V vs. Li/Li^+) at a scan rate of 0.1 mV sec^{-1}. The detailed information about optimization design is described in Figure S9–S12.

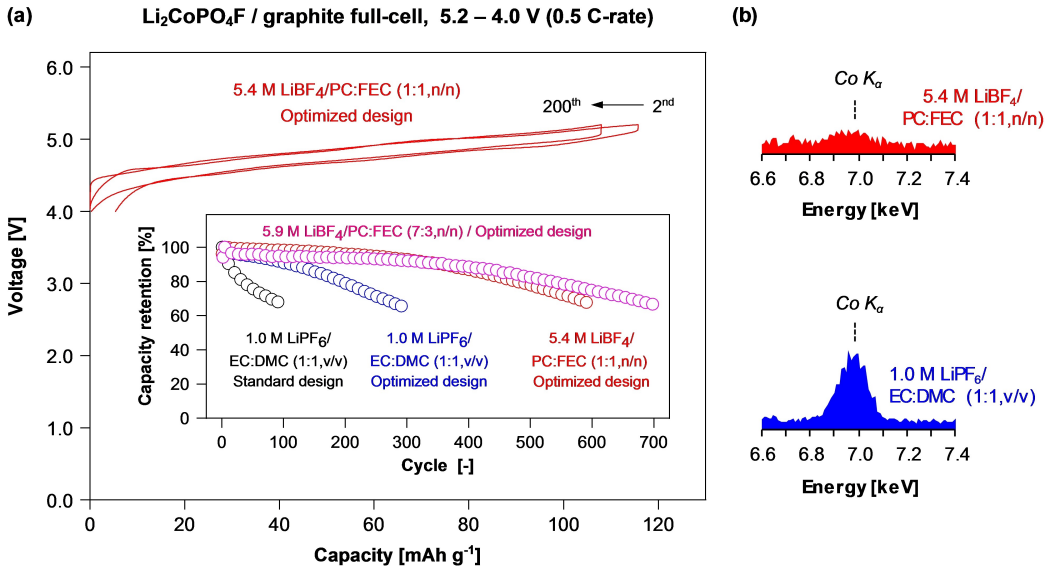

Figure 5. Highly reversible Li_2CoPO_4F/natural graphite full-cell with the concentrated $LiBF_4$/PC:FEC electrolyte. a) Charge and discharge curves of the cell with the optimized design and 5.4 M $LiBF_4$/PC:FEC (1:1, n/n) electrolyte. The inset demonstrates the superior discharge capacity retention of the optimized full-cell with concentrated $LiBF_4$/PC:FEC electrolytes compared with the standard or optimized design with the commercial electrolyte. b) EDX spectra of the graphite anodes collected from the Li_2CoPO_4F/natural graphite full-cells after 200 cycles with 5.4 M $LiBF_4$/PC:FEC (1:1, n/n) and 1.0 M $LiPF_6$/EC:DMC (1:1, v/v) electrolytes. In the optimized cell design, the cathode consisted of 85 wt% Li_2CoPO_4F/annealed AB composite, 10 wt% annealed AB, and 5 wt% LiPAA binder, and TEOS was applied to obtain a 5 wt% SiO_2-coated cathode. The vacuum drying conditions of the cathode were 200 °C for 1 h under vacuum. A heated quartz fiber was used as a separator. The loading level of the cathodes was 1.3–2.2 mg cm^{-2}. The N/P ratio was controlled between 1.3–1.4 based on the theoretical capacity of Li_2CoPO_4F (143.5 mAh g^{-1}; one Li^+) and graphite (372 mAh g^{-1}). The first charge-discharge curve is shown in Figure S12–13. The discharge capacities and Coulombic efficiencies upon cycling are shown in Figure S14.

surface corrosion of the Li_2CoPO_4F cathode.[52] In addition, even if the surface of the cathode is damaged, multi-valent transition metal complexes are difficult to form and migrate to the anode, because the concentrated electrolyte forms an AGG-predominant solution structure without free PC molecules that can readily solvate the complexes.[13]

3. Conclusions

A highly reversible 4.8 V Li_2CoPO_4F/graphite full-cell (with a 5.2 V cut-off) was successfully developed with concentrated $LiBF_4$/PC:FEC electrolytes in combination with a new cell design. The achieved cycling performance was the best for the Li_2CoPO_4F/graphite full-cell and was even better than that of Li_2CoPO_4F/Li half-cells in previous publications (Table S1). The simple design policies of the electrolyte enable overcoming the severe problems that have previously been encountered in developing 5 V-class batteries; (i) the high oxidation stability inherent to $LiBF_4$ salt and the unique solution structure inherent to the high concentration significantly reduce parasitic reactions that would otherwise occur at high-voltage region, and (ii) the high reduction stability provided by FEC-based SEI enables extremely stable cycling of the graphite anode without parasitic electrolyte decomposition and structural degeneration by the co-intercalation of solvent. Lastly, it is crucial to carefully study and optimize all cell components and procedures to achieve the stable cycling of high-voltage batteries. The dramatically improved cycling performance with our cell design indicates that previously reported poor cycling performance of such high-potential cathodes was indeed not originated only from the material or electrolyte itself, but also from other cell components. The design principles of electrolytes and other cell components presented here will motivate researchers to revisit various high-potential cathodes, which have been discarded due to poor cycling performance.

Experimental Section

Synthesis of Li_2CoPO_4F/C composites

Li_2CoPO_4F/C composites were synthesized *via* a modified multistep synthesis process based on the previous literature.[46] All chemicals were purchased from WAKO and used without any further purification.

$LiCoPO_4$: $LiCoPO_4$ was first synthesized with a sol-gel method. Briefly, $LiNO_3$, $Co(NO_3)_2{\cdot}6H_2O$, $NH_4H_2PO_4$, and citric acid were dissolved in deionized water with a molar ratio of 1:1:1:2 and vigorously stirred at 90 °C for several hours. Then, the mixture was dried at 120 °C overnight in an air oven. The obtained gel-like components were annealed at 350 °C for 3 hours to remove all volatile components. The intermediate powders were ground and pressed into pellets. The $LiCoPO_4$ product was successfully obtained by calcinating the pellets at 800 °C for 12 hours.

Li_2CoPO_4F: To prepare Li_2CoPO_4F, $LiCoPO_4$ was mixed with LiF at a rotational speed of 500 rpm for 10 hours using a ball-miller (Fritsch Pulverisette). The precursor of Li_2CoPO_4F was sealed in a silver tube in an Ar-filled glove box and heated at 650–700 °C for 5 hours with rapid quenching in water.

Li_2CoPO_4F/C: Li_2CoPO_4F/C composites were prepared by milling the Li_2CoPO_4F and carbon powders (pristine or annealed acetylene black; see the section below) at a weight ratio of 90:10, followed by annealing at 400 °C for 1 hour under an Ar flow.

Preparation of the electrolytes and cell components

Electrolyte : $LiBF_4$, lithium bis(fluorosulfonyl)amide (LiFSA), PC, FEC, ethylene carbonate (EC), dimethyl carbonate (DMC), and commercial 1.0 M $LiPF_6$/EC:DMC (1:1, v/v) electrolyte were purchased from Kishida Chemical as battery grade and used without further purification. The $LiBF_4$-based electrolytes and LiFSA-based electrolytes were prepared by mixing a given amount of salt with solvents in an Ar-filled glove box.

Conductive carbon: Two types of carbon conductive agents, pristine acetylene blacks (Li400, Denka Black) and annealed acetylene blacks were prepared. For the annealed sample, the pristine acetylene black was heated at 1100 °C for 5 hours under Ar atmosphere to remove the oxygen functional groups and impurities on the carbon surface.[45]

Binder: Commercial polyvinylidene difluoride (PVDF) and sodium carboxymethyl cellulose (NaCMC) binders were purchased from Kureha and Daicel Fine Chem Ltd., respectively, and used as received. LiPAA was prepared by titrating the PAA (Wako, molecular weight = 250,000) solution with LiOH (Wako) until a pH of 7 was obtained.

Separator: Four types of separators, polypropylene (PP3501, Celgard, denoted as PP), cellulose (Nippon Kodoshi), glass fiber (GFC, Advantec), and binderless quartz fiber (QR100, Advantec) were used in this experiment. The PP (60 °C), cellulose (120 °C), and glass fiber (120 °C) separators were dried overnight at a certain temperature under vacuum. The quartz separators were treated with thermal modification at 800–1000 °C under an Ar atmosphere for 5 hours. All prepared separators were stored in an Ar-filled glove box before assembling the cell.

Coin cell: The 2032-type standard coin cell parts (Al-clad positive case, stainless steel negative case, spring, and spacer with polypropylene O-ring) were purchased from Hohsen and dried overnight at 120 °C under vacuum, except for the polypropylene O-ring. The prepared cell parts were stored in an Ar-filled glove box before assembling the cell.

Preparation of the electrodes and coin cells

Li_2CoPO_4F electrode: The slurry of 85 wt% Li_2CoPO_4F/C composite with 10 wt% pristine or annealed acetylene black, and 5 wt% binder was mixed in deionized water, followed by the addition of TEOS (Wako) to obtain a 5 wt% SiO_2-coated electrode, and mixed again with a planetary centrifugal mixer (AR-100, Thinky Mixer) at 2000 rpm for several minutes. The prepared slurry was cast on a carbon-coated Al foil (SDX-PM, Showa Denko), dried at 60 °C in an air oven, and then pressed.

Graphite electrode: The graphite electrodes were fabricated by casting a slurry of 90 wt% natural graphite (SNO10, SEC Carbon) and 10 wt% PVDF binder in *N*-methyl pyrrolidone (Kanto Chemical) onto a Cu foil (Fchikawa Rare Metal) and dried at 60 °C in an air oven.

The electrodes were dried before their assembly into cells at 200 °C for 1 hour or 120 °C for 12 hours for cathodes, and 120 °C overnight for anodes under vacuum. The coin half-cells and full-cells were assembled in a glove box under Ar atmosphere.

Electrochemical study

All electrochemical measurements were performed at room temperature. Linear sweep voltammetry (LSV) was conducted to evaluate the anodic limits of the electrolytes with three-electrode cells consisting of a Pt plate as a working electrode and Li metal as the reference and counter electrodes, starting from the open circuit potential to 7 V (*vs.* Li/Li^+) at a scan rate of 0.1 $mV\,s^{-1}$. The VMP3 potentiostat (BioLogic) was used for the LSV measurement. The charge-discharge tests of the coin cells were conducted using a TOSCAT-3100 charge-discharge machine (Toyo System) with the given conditions.

Characterization

The basic physicochemical properties of the electrolytes are shown in Figure S1–S2. The viscosity of the electrolytes was determined with a viscometer (LoVis 2000 M, Anton Paar GmbH). The ionic conductivity was evaluated in a two-electrode cell (Pt|electrolyte|Pt) with AC impedance spectroscopy at 1 kHz (Solartron 147055BEC, Solartron Analytical).

Raman spectroscopy was applied to study the solution structure of the electrolytes with an NRS-5100 spectrometer (JASCO) at a laser excitation of 532 nm. To avoid any contamination from the air, the solutions were sealed in quartz cells under Ar atmosphere.

The transition metals deposited on the cycled graphite electrodes in the Li_2CoPO_4F/graphite full-cells after charge and discharge tests were analyzed by EDX. For the EDX measurement, the electrodes were collected from the cycled cells and rinsed several times with the DMC solvent in an Ar-filled glove box.

Acknowledgements

S.K. and Y.Y. proposed the concept. S.K. conducted the experiments and analyzed the data. S.K., Y.Y. and A.Y. contributed to the discussion and wrote the manuscript. A.Y. supervised the whole project. This work is supported by the JSPS KAKENHI Grant-in-Aid for Specially Promoted Research (Grant Number JP15H05701) and JSPS KAKENHI Grant-in-Aid for JSPS Fellows (Grant Number 17J10359).

Conflict of Interest

The authors declare no conflict of interest.

Keywords: High-voltage Li-ion batteries · Concentrated electrolytes · Wide potential windows · Cell design

[1] M. Armand, J.-M. Tarascon, *Nature* **2008**, *451*, 652–657.
[2] D. Larcher, J. M. Tarascon, *Nat. Chem.* **2015**, *7*, 19–29.
[3] J. W. Choi, D. Aurbach, *Nat. Rev. Mater.* **2016**, *1*, 16013.
[4] A. Kraytsberg, Y. Ein-Eli, *Adv. Energy Mater.* **2012**, *2*, 922–939.
[5] M. Hu, X. Pang, Z. Zhou, *J. Power Sources* **2013**, *237*, 229–242.
[6] C. M. Julien, A. Mauger, *Ionics* **2013**, *19*, 951–988.
[7] W. Li, B. Song, A. Manthiram, *Chem. Soc. Rev.* **2017**, *46*, 3006–3059.
[8] S. Tan, Y. J. Ji, Z. R. Zhang, Y. Yang, *ChemPhysChem.* **2014**, *15*, 1956–1969.

[9] M. He, L. Hu, Z. Xue, C. C. Su, P. Redfern, L. A. Curtiss, B. Polzin, A. Von Cresce, K. Xu, Z. Zhang, *J. Electrochem. Soc.* **2015**, *162*, A1725–A1729.
[10] Z. Zhang, L. Hu, H. Wu, W. Weng, M. Koh, P. C. Redfern, L. A. Curtiss, K. Amine, *Energy Environ. Sci.* **2013**, *6*, 1806–1810.
[11] L. Chen, X. Fan, E. Hu, X. Ji, J. Chen, S. Hou, T. Deng, J. Li, D. Su, X. Yang, C. Wang, *Chem.* **2019**, *5*, 896–912.
[12] Y. Yamada, A. Yamada, *J. Electrochem. Soc.* **2015**, *162*, A2406–A2423.
[13] J. Wang, Y. Yamada, K. Sodeyama, C. H. Chiang, Y. Tateyama, A. Yamada, *Nat. Commun.* **2016**, *7*, 12032.
[14] T. Doi, Y. Shimizu, M. Hashinokuchi, M. Inaba, *J. Electrochem. Soc.* **2016**, *163*, A2211–A2215.
[15] T. Doi, Y. Shimizu, M. Hashinokuchi, M. Inaba, *ChemElectroChem.* **2017**, *4*, 2398–2403.
[16] T. Doi, Y. Shimizu, R. Matsumoto, M. Hashinokuchi, M. Inaba, *ChemistrySelect.* **2017**, *2*, 8824–8827.
[17] J. Wang, Y. Yamada, K. Sodeyama, E. Watanabe, K. Takada, Y. Tateyama, A. Yamada, *Nat. Energy* **2018**, *3*, 22–29.
[18] J. Alvarado, M. A. Schroeder, M. Zhang, O. Borodin, E. Gobrogge, M. Olguin, M. S. Ding, M. Gobet, S. Greenbaum, Y. S. Meng, K. Xu, *Mater. Today* **2018**, *21*, 341–353.
[19] L. Suo, W. Xue, M. Gobet, S. G. Greenbaum, C. Wang, Y. Chen, W. Yang, Y. Li, J. Li, *Proc. Natl. Acad. Sci. USA* **2018**, *115*, 1156–1161.
[20] S. Ko, Y. Yamada, K. Miyazaki, T. Shimada, E. Watanabe, Y. Tateyama, T. Kamiya, T. Honda, J. Akikusa, A. Yamada, *Electrochem. Commun.* **2019**, *104*, 106488.
[21] J. Qian, W. A. Henderson, W. Xu, P. Bhattacharya, M. Engelhard, O. Borodin, J. G. Zhang, *Nat. Commun.* **2015**, *6*, 6362.
[22] Y. Yamada, K. Usui, C. H. Chiang, K. Kikuchi, K. Furukawa, A. Yamada, *ACS Appl. Mater. Interfaces* **2014**, *6*, 10892–10899.
[23] K. Sodeyama, Y. Yamada, K. Aikawa, A. Yamada, Y. Tateyama, *J. Phys. Chem. C* **2014**, *118*, 14091–14097.
[24] Y. Yamada, C. H. Chiang, K. Sodeyama, J. Wang, Y. Tateyama, A. Yamada, *ChemElectroChem.* **2015**, *2*, 1687–1694.
[25] F. Kita, H. Sakata, S. Sinomoto, A. Kawakami, H. Kamizori, T. Sonoda, H. Nagashima, J. Nie, N. V. Pavlenko, Y. L. Yagupolskii, *J. Power Sources* **2010**, *90*, 27–32.
[26] T. Doi, Y. Shimizu, M. Hashinokuchi, M. Inaba, *J. Electrochem. Soc.* **2017**, *164*, A6412–A6416.
[27] S. S. Zhang, K. Xu, T. R. Jow, *J. Electrochem. Soc.* **2002**, *149*, A586–A590.
[28] J. L. Allen, O. Borodin, D. M. Seo, W. A. Henderson, *J. Power Sources* **2014**, *267*, 821–830.
[29] D. M. Seo, P. D. Boyle, J. L. Allen, S.-D. Han, E. Jónsson, P. Johansson, W. A. Henderson, *J. Phys. Chem. C* **2014**, *118*, 18377–18386.
[30] K. Yoshida, M. Nakamura, Y. Kazue, N. Tachikawa, S. Tsuzuki, S. Seki, K. Dokko, M. Watanabe, *J. Am. Chem. Soc.* **2011**, *133*, 13121–13129.
[31] O. Borodin, W. Behl, T. R. Jow, *J. Phys. Chem. C* **2013**, *117*, 8661–8682.
[32] K. Xu, *Chem. Rev.* **2004**, *104*, 4303–4417.
[33] S. K. Jeong, M. Inaba, Y. Iriyama, T. Abe, Z. Ogumi, *Electrochem. Solid-State Lett.* **2003**, *6*, A13.
[34] M. Nie, D. P. Abraham, D. M. Seo, Y. Chen, A. Bose, B. L. Lucht, *J. Phys. Chem. C* **2013**, *117*, 25381–25389.
[35] P. C. Shi, M. Lin, H. Zheng, X. D. He, Z. M. Xue, H. F. Xiang, C. H. Chen, *Electrochim. Acta.* **2017**, *247*, 12–18.
[36] Y. Yamada, K. Furukawa, K. Sodeyama, K. Kikuchi, M. Yaegashi, Y. Tateyama, A. Yamada, *J. Am. Chem. Soc.* **2014**, *136*, 5039–5046.
[37] K. Sodeyama, Y. Yamada, K. Aikawa, A. Yamada, Y. Tateyama, *J. Phys. Chem. C* **2014**, *118*, 14091–14097.
[38] H. Moon, R. Tatara, T. Mandai, K. Ueno, K. Yoshida, N. Tachikawa, T. Yasuda, K. Dokko, M. Watanabe, *J. Phys. Chem. C* **2014**, *118*, 20246–20256.
[39] H. Moon, T. Mandai, R. Tatara, K. Ueno, A. Yamazaki, K. Yoshida, S. Seki, K. Dokko, M. Watanabe, *J. Phys. Chem. C* **2015**, *119*, 3957–3970.
[40] S. Chen, J. Zheng, D. Mei, K. Sung Han, M. H. Engelhard, W. Zhao, W. Xu, J. Liu, J.-G. Zhang, S. Chen, J. Zheng, W. Zhao, W. Xu, J. Liu, J. Zhang, D. Mei, K. S. Han, M. H. Engelhard, *Adv. Mater.* **2018**, *30*, 17061021.
[41] N. P. W. Pieczonka, V. Borgel, B. Ziv, N. Leifer, V. Dargel, D. Aurbach, J. H. Kim, Z. Liu, X. Huang, S. A. Krachkovskiy, G. R. Goward, I. Halalay, B. R. Powell, A. Manthiram, *Adv. Energy Mater.* **2015**, *5*, 1501008.
[42] R. Sharabi, E. Markevich, V. Borgel, G. Salitra, D. Aurbach, G. Semrau, M. A. Schmidt, N. Schall, C. Stinner, *Electrochem. Commun.* **2011**, *13*, 800–802.
[43] C. L. Campion, W. Li, B. L. Lucht, *J. Electrochem. Soc.* **2005**, *152*, A2327-A2334.
[44] J. S. Gnanaraj, E. Zinigrad, L. Asraf, H. E. Gottlieb, M. Sprecher, M. Schmidt, W. Geissler, D. Aurbach, *J. Electrochem. Soc.* **2003**, *150*, A1533–A1537.
[45] S. Ko, Y. Yamada, L. Lander, A. Yamada, *Carbon* **2020**, *158*, 766–771.
[46] T. Okumura, M. Shikano, Y. Yamaguchi, H. Kobayashi, *Chem. Mater.* **2015**, *27*, 2839–2847.
[47] C. Chang, Z. Huang, R. Tian, X. Jiang, C. Li, J. Feng, *J. Power Sources* **2017**, *364*, 351–358.
[48] S. Amaresh, G. J. Kim, K. Karthikeyan, V. Aravindan, K. Y. Chung, B. W. Cho, Y. S. Lee, *Phys. Chem. Chem. Phys.* **2012**, *14*, 11904–11909.
[49] D. Wang, J. Xiao, W. Xu, Z. Nie, C. Wang, G. Graff, J. G. Zhang, *J. Power Sources* **2011**, *196*, 2241–2245.
[50] N. R. Khasanova, A. N. Gavrilov, E. V. Antipov, K. G. Bramnik, H. Hibst, *J. Power Sources* **2011**, *196*, 355–360.
[51] S. S. Fedotov, A. A. Kabanov, N. A. Kabanova, V. A. Blatov, A. Zhugayevych, A. M. Abakumov, N. R. Khasanova, E. V. Antipov, *J. Phys. Chem. C.* **2017**, *121*, 3194–3202.
[52] R. Younesi, G. M. Veith, P. Johansson, K. Edström, T. Vegge, *Energy Environ. Sci.* **2015**, *8*, 1905–1922.

Manuscript received: March 6, 2020
Revised manuscript received: April 13, 2020
Version of record online: May 13, 2020